ELECTROSPUN SCAFFOLDS FOR WOUND HEALING APPLICATIONS FROM POLY(4-HYDROXYBUTYRATE): A BIOBASED AND BIODEGRADABLE LINEAR POLYMER WITH HIGH ELASTOMERIC PROPERTIES

Ina Keridou[1], Lourdes Franco[1,2], Juan C. Martínez[3], Pau Turon[4], Luis J. del Valle,[1,2] Jordi Puiggalí[1,2]

[1]Departament d'Enginyeria Química, Universitat Politècnica de Catalunya, Escola d'Enginyeria de Barcelona Est-EEBE, c/Eduard Maristany 10-14, Barcelona 08019, SPAIN

[2]Barcelona Research Center for Multiscale Science and Engineering, Universitat Politècnica de Catalunya, Escola d'Enginyeria de Barcelona Est-EEBE, Barcelona 08019, SPAIN

[3]ALBA Synchrotron Light Facility, Carrer de la Llum, 2-26, 08290, Cerdanyola del Vallès, Barcelona, SPAIN

[4]B. Braun Surgical, S.A.U. Carretera de Terrasa 121, 08191 Rubí (Barcelona), SPAIN

ABSTRACT

Electrospun scaffolds of the biodegradable and biocompatible poly-4-hydroxybutyrate (P4HB) polyester have been prepared using horizontal and vertical set-up configurations of electro-spinning. Specifically, it has been evaluated the influence of solvent, polymer concentration, and processing parameters, such as applied voltage, flow rate, and needle tip-collector distance. Scaffolds obtained under the most favorable conditions were characterized in terms of crystallinity, lamellar supramolecular order, thermal (including calorimetric and thermogravimetric data), mechanical and surface properties. Results pointed out significant differences with respect to commercial sutures (based in P4HB, e.g., MonoMax®) and demonstrated that electrospun scaffolds were constituted by crystalline microfibers with a tangled distribution that leads to both high modulus and elasticity. Furthermore, new scaffolds had thermal stability and a rough surface that led to a hydrophobic character. Scaffolds could also be successfully loaded during the electrospinning process with a peptide analog to the fibroblast growth factor (e.g., CYRSRKYSSWYVALKRC), giving rise to fully biocompatible samples with a clear acceleration in wound healing.

Keywords: Poly(4-hydroxybutyrate), biodegradable polymers, electrospinning, scaffolds, wound healing, fibroblast growth factor.

INTRODUCTION

Poly(4-hydroxybutyrate) (P4HB) is a biodegradable polyester belonging to the polyhydroxyalkanoates family (PHA), which can be obtained with a high yield from microorganisms (e.g., *Escherichia coli* K12) [1] in response to physiological stress conditions. Limitation of nutrients is probably the main mechanism to induce the production of P4HB, as it is also reported for other poly(hydroxyalkanoates) [2]. P4HB has exceptional mechanical properties considering its high elongation at break, which is not comparable with related linear polyesters with even number of carbon atoms in the main chain of the repeat unit. These are derived from condensation of ω-hydroxy acids or alternatively from ring opening polymerization of glycolide and lactones, and correspond to poly(glycolic acid) or polyglycolide and poly(6-hydroxyhexanoic acid) or poly(ε-caprolactone) (i.e., polymers with two and six carbon atoms instead of the four atoms of P4HB).

P4HB is hydrolyzed in the body under the action of water and enzymes to 4-hydroxybutyric acid, which is found within a variety of tissues of mammalians (e.g., brain, heart, kidney, liver, lung, muscles). The monomer can be quickly metabolized in the body, with a reported half-life time close to 30 minutes [3].

Nowadays P4HB has wide biomedical applications due to its biocompatibility, biodegradability and mechanical properties. TephaFLEX®, MonoMax®, BioFiber™, Phasix™ and GalaFLEX are commercial trademarks of P4HB based materials used in medical devices, such as abdominal wall closure materials, long-term bioresorbable sutures, tendon repair scaffolds, hernia repair meshes and reconstructive surgery materials [1,4-8].

Porous scaffolds constituted by knitted P4HB monofilament fibers (diameter close to 40 μm) provided a durable mechanical reinforcement of soft tissue, according to both *in vitro* and *in vivo* assays [9]. A 50% of its initial strength could be retained over 12 weeks after implantation and the device could be fully resorbed within 12 to 18 months.

Electrospinning is currently one of the most popular processes for preparing nonwoven micro- and nanofibers arranged into porous scaffolds [9-11]. This process uses electrostatic forces (10–100 kV) to stretch drops of a polymer dilute solution from a needle tip to a collector. Applications in the biomedical field are extensive [12-14] due to a combination of factors that include economic feasibility, easiness of preparation and high versatility. Incorporation of drugs into electrospun scaffolds can also be easily performed, with minimum changes being usually required from the optimized processing conditions determined for building the polymer matrix. The repercussions on the final fiber geometry are usually low even when several drugs are incorporated to provide multifunctional properties [15].

Electrospinning has been widely applied for the preparation of scaffolds based on poly(hydroxyalkanoates), such as poly(3-hydroxybutyrate) (P3HB) and poly(3-hydroxyvalerate) [16,17]. Thus, properties of the rigid P3HB can be improved after being electrospun due to the decrease on its degree of crystallinity. In addition, an increase on the biodegradation rate and an improvement of interactions with tissue cells were also observed [16]. Copolymers of 3HB and 4HB have also been satisfactorily electrospun [18], but surprisingly, no specific study has been performed with the related and linear P4HB homopolymer.

The FGF-2 protein is a powerful pluripotent Fibroblast Growth Factor (FGF) that is also relevant for being the first angiogenic protein obtained from a tumor [19]. This protein prevents cell depletion by differentiation and apoptosis, and it is implicated in wound healing

and angiogenesis processes [20]. FGF-P is a synthetic analogue that can also bind to the fibroblast growth factor receptor. This mimetic polypeptide is based on a 15-amino acid region with order: CYRSRKYSSWYVALKRC that is also present in the natural FGF-2 protein. On the other hand, FGF-P has the advantage, with respect to other growth factors, to cause a minimum inflammation or vascular leakage. Furthermore, it enhances the formation of new blood vessels in angiogenesis and improves bone growth [21].

Main goals of the present work focus on the evaluation of the polymer solution conditions, processing parameters and optimal experimental set-up configurations to produce suitable P4HB scaffolds by electrospinning. Furthermore, the conditions for loading the FGF-P growth factor into a representative electrospun scaffold will also be determined to assess its wound healing effect.

EXPERIMENTAL SECTION

Materials

Commercially available samples of P4HB (MonoMax®) were kindly supplied by B. Braun Surgical S.A.U. Weight and number average molecular weights of P4HB samples were 215,000 and 68,000 g/mol, as determined by GPC [22]. The synthetic FGF-P peptide had a purity of 93%, a molecular weight of 2,170 g/mol and was purchased from GenScript (Piscataway, NJ, USA). Saos-2 cells (ATCC® HTB-85™, ephithelial cells derived from human osteosarcoma) and NRK-49F cells (ATCC® CRL-1570™, fibroblast cells derived from rat kidney, *Rattus norvegicus*) both of growth adherent were purchased from ATCC (American Type Culture Collection, Manassas, VA, USA).

Preparation of neat and FGF-P loaded electrospun scaffolds

Electrospinning was carried out in a non-conductor cabinet. Polymer solutions were loaded in a 10 mL BD Discardit (Becton Dickson Co., Franklin Lakes, NJ, USA) plastic syringe for

delivery through a blunt-tipped (i.e., without bevel) 23 G needle (inner diameter 0.64 mm). The prepared solutions were delivered via a single KDS100 infusion syringe pump (KD Scientific, USA) to control the flow rate (from 1 to 5 mL h^{-1}). Electrospun fibers were deposited to both a flat and a rotatory collector placed at different distances (10–25 cm) from the needle tip, which was vertically and horizontally oriented, respectively (Figure 1). A high voltage supply (Gamma High Voltage Research, ES30−5W) was applied to the selected collector. All electrospinning experiments were carried out at room temperature.

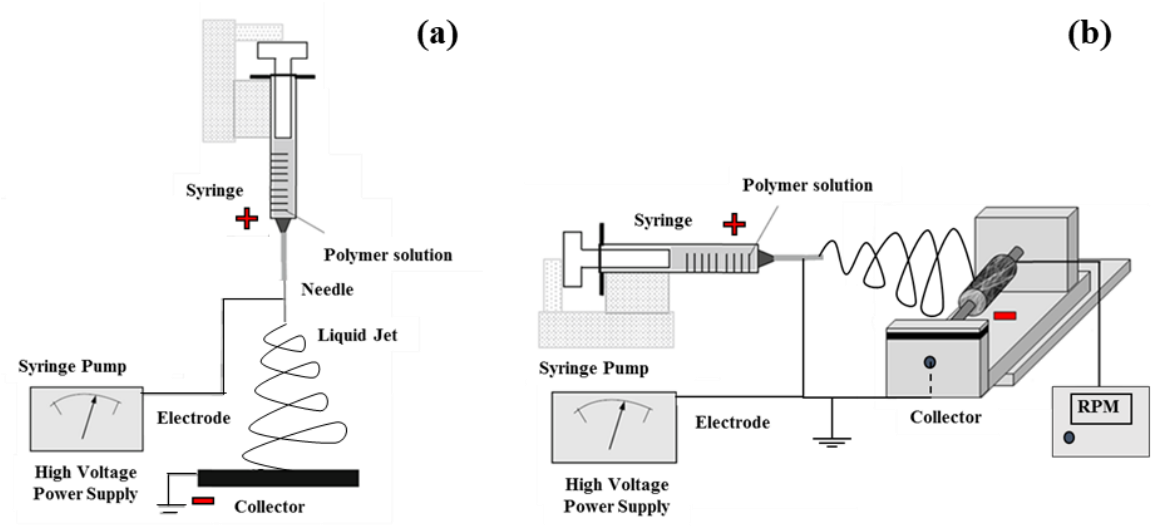

Figure 1. Schematic diagrams of the employed electrospinning equipment: (a) Vertical disposition with a planar collector surface, (b) Horizontal disposition with a rotating cylinder collector.

Neat and FGF-P loaded electrospun fibers were prepared using optimized parameters (i.e., collector distance, voltage, and flow rate) and dissolution conditions (i.e., solvent and concentrations of polymer and polymer/polypeptide).

Fiber morphology was firstly surveyed by optical microscopy using a Zeiss Axioskop 40 optical microscope equipped with a Zeiss AxioCam MRC5 digital camera. Accurate morphologic analysis was carried out by scanning electron microscopy (SEM) using a Phenom XL Desktop SEM equipment. Fibrous mats, which were cut in 1 cm × 1 cm samples, were mounted on a double-sided adhesive carbon disc and were sputter-coated with a thin

layer of carbon to prevent sample charging problems using a K950X Turbo Evaporator. All samples were observed at an accelerating voltage of 15 kV. Diameters of electrospun microfibers were measured with the SmartTiff software from Carl Zeiss SMT, Ltd.

Measurements of physical properties of electrospun scaffolds

Calorimetric data were obtained by differential scanning calorimetry with a TA Instruments Q100 series equipped with a refrigerated cooling system (RCS) operating at temperatures from -80 ºC to 400 ºC. Calibration was performed with indium. Experiments were conducted under a flow of dry nitrogen with a sample weight of approximately 5 mg. Calorimetric data were obtained from runs performed at heating rate of 10 ºC/min.

The thermal stability of the P4HB samples was studied by thermogravimetric analysis (TGA) at a heating rate of 10 ºC/min (sample weight *ca.* 5 mg) with a Q50 thermogravimetric analyzer of TA Instruments and under a flow of dry nitrogen. Test temperatures ranged from 30 to 600 ºC.

WAXD and SAXS patterns were taken simultaneously employing the 16 bits-CCD Rayonix LX255-HS and 20 bits-single photon counter Dectris Pilatus 3s 1M detectors respectively. The experiment was performed at the NCD-SWEET beamline (BL11) of the ALBA synchrotron facility (Cerdanyola del Vallès, Barcelona, Spain), by using a photon wavelength of 0.100 nm. Polymer samples were confined between Kapton films. WAXD and SAXS diffraction patterns were calibrated with Cr_2O_3 and silver behenate (AgBh), respectively. The correlation function and the corresponding parameters were calculated with the CORFUNC software for Fibre Diffraction/Non-Crystalline Diffraction provided by the Collaborative Computational Project 13. Deconvolution of WAXD peaks was performed using the PeakFit 4.0 software.

Contact angle (CA) measurements were conducted using the sessile drop method. 0.5 µL of milliQ water drops were deposited onto the surface of the electrospun mats, which were cut

into rectangular pieces (3 cm x 1 cm) and fixed on a holder, and recorded after stabilization with the equipment OCA 15EC (DataPhysics Instruments GmbH, Filderstadt). The SCA20 software was used to measure the CA, which is shown here as the average of at least 40 measures for each condition.

Mechanical properties were determined with a Zwick Z2.5/TN1S (Zwick/Roell; Ulm, Germany) testing machine in stress-strain tests carried out at a deformation rate of 10 mm/min. The load cell capacity was 100 N. Mechanical parameters were evaluated by means of the testXpert software of Zwick. In the case of the elastic modulus calculation, force values were delimited to the lineal part of the representation. Measurements were performed on rectangular samples of 3 cm × 0.4 cm and a width of 0.40 mm that were cut from the collected electrospun scaffolds. The mechanical parameters were averaged from a minimum of six measurements for each polymer sample.

Cell adhesion and proliferation assays

Studies were performed with fibroblast NRK cells and epithelial Saos-2 cells. In all cases, cells were cultured in Dulbecco's Modified Eagle Medium (DMEM) with 4500 mg/L of glucose, 110 mg/L of sodium pyruvate and 2 mM of L-glutamine) supplemented with 10% fetal bovine serum (FBS), 50 U/mL penicillin, 50 mg/mL streptomycin and L-glutamine 2 mM at 37 ºC in a 10% humidified atmosphere of 5% CO_2 and 95% air. Culture media were changed every two days. For sub-culture, cell monolayers were rinsed with PBS and detached by incubating them with 0.25% trypsin/EDTA for 2-5 min at 37 ºC. The incubation was stopped by suspending in 5 mL of fresh medium and the cell concentration was determined by counting with Neubauer camera and using 4% trypan blue as dye vital.

Square pieces of neat and FGF-P loaded electrospun scaffolds (1 cm x 1 cm x 0.40 mm) were placed and fixed in each well of a 24-well culture plate with a small drop of silicone

(Silbione® MED ADH 4300 RTV, Bluestar Silicones France SAS, Lyon, France). This plate was then sterilized by UV-radiation in a laminar flux cabinet for 15 min. For cell adhesion assays, aliquots of 50–100 μL containing 5×10^4 cells were seeded onto the scaffold samples in each well and incubated for 24 h (adhesion assay). For cell proliferation assays, the same aliquot volume but containing a lower cell concentration than that for adhesion experiments (i.e., 2×10^4 cells) was seeded and incubated for 96 h. Adhesion and proliferation in the samples were evaluated to obtained quantitative data by the MTT method [23]. The procedure is based on a simple modification of the ISO10993–5:2009 standard test, which describes the appropriate methodology to assess *in vitro* cytotoxicity of medical devices. This test is designed to determine the *in vitro* biological response of mammalian cells using appropriate biological parameters. According to this ISO standard, devices fall into one of three categories based on expected contact with the patient: (a) Limited (≤24 h), (b) Prolonged (>24 h and ≤30 days) and (c) Permanent (>30 days). In our case, the assay was performed according to the limited and prolonged categories. The viability results were averaged after doing four replicates. Samples with adhered and grown cells were fixed with 2.5 w/v-% formaldehyde at 4°C overnight. They were subsequently dehydrated and processed for observation of cell morphology using fluorescence microscopy, where the nucleus and actin cytoskeleton were stained with Hoescht and phalloidin, respectively.

In-vitro wound healing activity of FGF-P

An *in-vitro* wound-healing cell migration assay was employed to evaluate the effect of FGF-P peptide loaded in the electrospun because FGF-P enhance proliferation and cell migration. Confluent monolayers of fibroblast NRK cells were obtained after 48 h of culture in 1 mL of DMEM medium containing 10^5 cells seeded in each well (24-well plate). Subsequently, a scratch (a linear defect to mimic a wound) was made in the

monolayers with a sterilized propylene tip (diameter of 0.2 mm) and the layer was rinsed with PBS to remove cells damaged during scratch formation. Then, 1 mL of medium was added to each well, together with a square piece of the FGF-P loaded electrospun scaffolds (1 cm x 1 cm x 0.40 mm) (five samples for each assay). Unloaded scaffolds were used as controls. The rate of healing was monitored using an inverted light microscope and taking micrographs every 24 h at the same magnification. The free area between cells was determined by fitting it to a rectangular geometry. The evolution of healing over time (*WH, wound healing*) was determined as:

$$WH\ (\%) = (A_0\text{-}At) / A_0 \times 100 \qquad (1)$$

where At and A_0 correspond to the areas evaluated at times t and 0, respectively. The micrographs were stitched successfully, so as to depict the evolution of the wound closure, by using the grid/collection stitching plugin available through ImageJ Fiji [24].

Statistical Analysis

Values were averaged and graphically represented together with their respective standard deviations. Statistical analysis was performed by one-way ANOVA test to compare the means of all groups, and then Tukey's test was applied to determine a statistically significant difference between two groups. The test confidence level was set at 95% ($p < 0.05$).

RESULTS AND DISCUSSION

Electrospinning of P4HB solutions

Electrospinning is a complex process where different forces are involved (e.g., fluid dynamics, electric force, Coulomb repulsion force, surface tension and gravity). Influence of gravity can be varied through the experimental set-up, therefore in this work both vertical and horizontal configurations are considered (Figure 1). Theoretically, gravity can increase

the effect of the applied electrical field and contribute to render thin fibers with a wide diameter size distribution [25].

The type of selected collector has also a great repercussion on the disposition of fibers in the electrospun scaffold. In this case, we have chosen a static plane collector for the vertical set-up and a rotatory collector, which should favour the alignment of fibers, for the horizontal disposition.

Selection of an appropriate solvent for a polymer with a determined chemical structure and molecular weight is fundamental to succeed in the production of micro/nanofibers electrospun [26]. However, correlation between solubility and spinnability is nevertheless problematic since in some cases it may be preferable to select a worse solvent to avoid formation of irregularities such as droplets and beads [27]. Thus, to test conditions using a set of solvents with relatively close solubility parameters (both typical Hildebrand [28] and Hansen [29] parameters can be considered) is fundamental.

The predicted solubility parameter of P4HB becomes higher than that determined for P3HB, which is the related and most common studied PHA, due to the different contribution of CH, CH_3 and CH_2 groups (57, 437 and 272 $MPa^{1/2}$ mL/mol, respectively). Therefore, values of 10.3 H and 9.3 H can be estimated for P4HB and P3HB, respectively, considering densities of 1.25 g/mL (P4HB) and 1.21 g/mL (P3HB). Abundant studies can be found concerning P3HB solubility [30] and electrospinnability [31, 32], which could be an adequate basis for selecting appropriate conditions for P4HB. The high molecular weight of P3HB produced by microbial biosynthesis was found problematic in some cases due to the high viscosity attained in determined solvents. For example, acetone (dry) showed some advantages with respect to chloroform (stabilized with amylene) as consequence of rendering a lower solution viscosity. However, chloroform is in general preferred due its closer solubility parameter with that estimated for P3HB (i.e., 9.24-9.29 H and 9.78-10.02

H are determined for chloroform and acetone, respectively) [31]. Nevertheless, some problems concerning the use of chloroform have been reported, being these mainly related to its low dielectric constant and boiling point, which could lead to a fast polymer crystallization, needle obstruction and noncontinuous processing. Addition of a small percentage of solvents with lower volatility, such as dimethylformamide, may be interesting to solve the mentioned difficulties.

In the present work, chloroform, chloroform/acetone mixture in a 2:1 *v*/*v* ratio, dichloromethane (DCM), tetrahydrofurane (THF) and 1,1,1,3,3,3-hexafluoroisopropanol (HIFP) have been selected as potential solvents. Hildebrand and Hansen solubility parameters of these solvents are summarized in Table 1. Reported dispersive, polar and hydrogen bond parameters for P3HB are 7.77, 3.27 and 4,79 $(cal/mL)^{1/2}$ [33], each value being intermediate between those reported in the Table. Note that acetone, dichloromethane and HFIP are the most appropriate considering the dispersive, polar and hydrogen bond contributions, respectively.

Table 1. Hildebrand and Hansen parameters of the assayed solvents [29, 32].

Solvent	**Hildebrand parameter** $(cal/mL)^{1/2}$	**Hansen parameters**[a)] **D-P-H** $(cal/mL)^{1/2}$
Chloroform	9.21	8.70-1.52-2.79
Dichloromethane	9.93	8.31-3.57-3.47
Acetone	9.77	7.58-5.08-3.42
Chloroform/ Acetone 2:1	9.40	8.31-2.69-3.00
Tetrahydrofurane	9.52	8.21-2.79-3.91
1,1,1,3,3,3-Hexafluoroisopropanol	8.74	8.41-2.20-7.19

[a)] Dispersive, polar and hydrogen bonding contributions are indicated by D, P, H, respectively.

The main study for the optimization of processing parameters (needle tip, collector distance, flow rate, applied voltage and polymer concentration) was performed with chloroform.

These parameters were the initial starting conditions for the study of the other solvents, with them being subsequently modified according to morphological observations by optical microscopy. Note that the maximum difference between Hildebrand parameters of the polymer and each solvent was less that 1.8 $(cal/mL)^{1/2}$, which is the maximum allowed value. Electrospinning experiments were planned to work with dissolutions having high polymer concentration and great flow rate in order to minimize the deposition time required to get a consistent scaffold. In general, high voltages were required due to the high viscosity of concentrated solutions and the high polymer molecular weight.

The vertical set-up configuration had as a main limitation the trend to produce drops in the collector due to an incomplete evaporation of the solvent in the fluid jet. Figures 2a and 2b show typical disks attained after solvent evaporation (chloroform) in the plate collector. Our observations indicated that these drops could be avoided by decreasing the flow rate and also by increasing the applied voltage, which strengthens the fluid jet. Additionally, note the reduction of the disk diameter according to the indicated decrease and increase of the flow rate and voltage, respectively.

The behavior of chloroform, dichloromethane, chloroform/acetone mixtures and THF was similar with specific differences that will then be explained. HFIP is a polar solvent with strong hydrogen bonding properties (i.e., the Hansen hydrogen bonding parameter becomes 7.19 $(cal/mL)^{1/2}$) that enables it to dissolve hydrogen-bond acceptors as P4HB despite the existing high discrepancy between Hildebrand solubility parameters (i.e., 1.56 $(cal/mL)^{1/2}$). In that event, main problems concern to the buckling instability of the fluid jet during deposition, which lead to circles, figures-of-eight, wavy fibers and meanders. Figure 2c depicts that nanosized fibers could be obtained from highly diluted solution, but even using a relatively high flow rate the formed wavy fibers had a clear trend to form aggregates.

Finally, high polymer concentrations lead to deficient solvent evaporation and a meander appearance (Figure 2d).

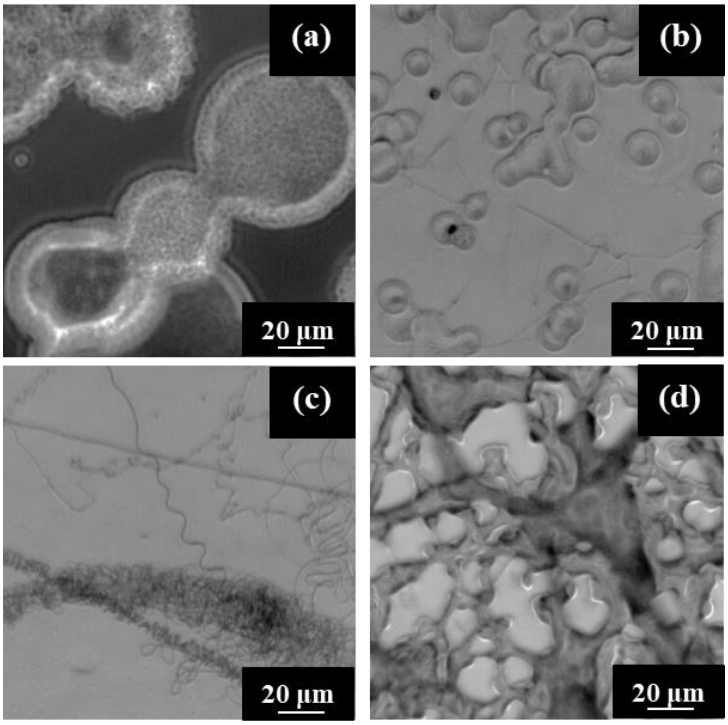

Figure 2. Optical micrographs showing typical defects attained with vertical electrospinning: (a, b) Disk morphologies, (c) wavy fiber agglomerates and (d) irregular planar fibers with solvent retention. Specific conditions: (a) 5 *w*/*v*-% in chloroform, 15 cm, 25 kV, 5 mL/h; (b) 8 *w*/*v*-% in chloroform, 16.5 cm, 40 kV, 2 mL/h; (c) 0.5 *w*/*v*-% in HFIP, 16.5 cm, 70 kV, 9 mL/h and (d) 15 *w*/*v*-% in HFIP, 16.5 cm, 70 kV, 2 mL/h.

Comparison of optical micrographs shown in Figures 3a and 3b illustrates as a general trend that an increment on the solvent flow rate (e.g., from 0.5 mL/h to 1.5 mL/h) required a higher voltage (e.g., 50 kV with respect to 70 kV) and a drastic decrease on the polymer concentration ((e.g., from 15 *w*/*v*-% to 9 *w*/*v*-%) in order to avoid drop formation and obtain homogeneous and continuous fibers.

The given example corresponds to chloroform, but similar conclusions were deduced for the other studied solvents. Figure 3c shows that the addition of acetone to chloroform allowed working with a very high polymer concentration (e.g., 15 *w*/*v*-%) and even a lower voltage (60 kV) and higher flow rate (3 mL/h) while keeping the same needle-collector distance

(16.5 cm). The change of chloroform (Figure 3b) by dichloromethane (Figure 3d) had also some advantages since the flow rate could be higher (5 mL/h with respect to 1.5 mL/h) whereas the voltage could be lower (50 kV respecting to 70 kV), when concentration and collector distance were maintained at the same values. THF was a highly problematic solvent since processing conditions were highly limited and for example the flow rate should be as lower as 0.5 mL/h for a concentration of 9 *w*/*v*-% (Figure 3e). Finally, and despite the above indicated problems, a high concentration (18 *w*/*v*-%) and moderate flow rate (4 mL/h) was possible when HFIP was selected (Figure 3f). Note however, the increase on the collector distance (up to 18.5 cm and the fact that fiber agglomeration could still be observed.

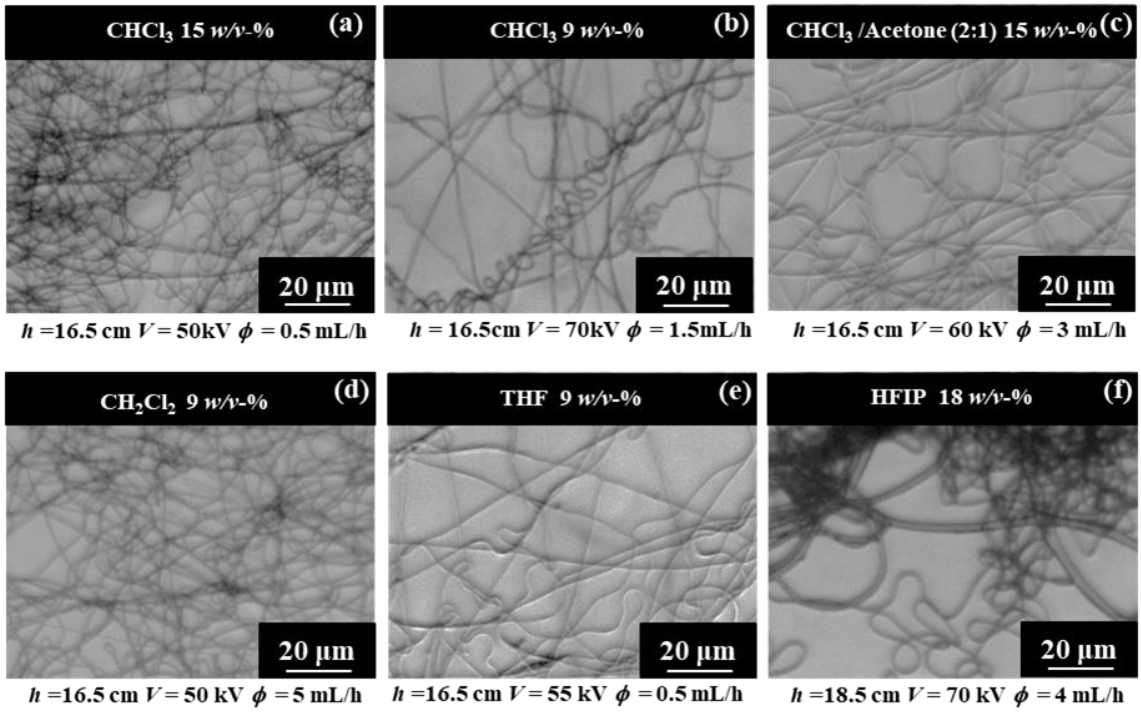

Figure 3. Optical micrographs showing electrospun fibers obtained with a vertical set up and the indicated solvent, polymer concentration, flow rate, voltage and collector distance.

SEM micrographs of the sample preparation obtained from chloroform with 9 *w*/*v*-% concentration showed the formation of continuous microfibers with a relatively narrow distribution (1.3 ± 0.5 μm) and a smooth surface (Figure 4). Higher diameters were attained

with the chloroform/acetone solvent mixture and dichloromethane as expected from the increased flow rate.

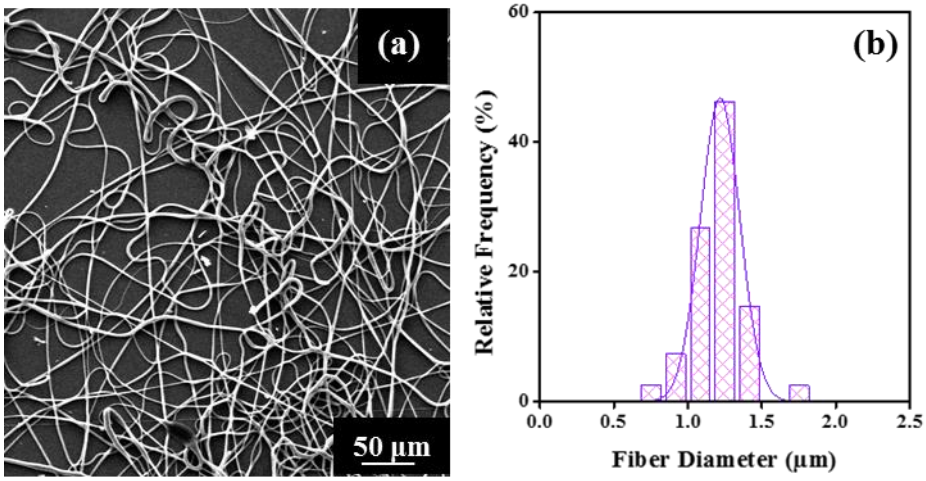

Figure 4. (a) Scanning electron micrograph of electrospun P4HB fibers prepared with a vertical set up from chloroform at a polymer concentration of 9 *w*/*v*-%, flow rate of 1.5 mL/h, voltage of 70 kV and tip-collector distance of 16.5 cm. (b) Diameter distribution of the electrospun fibers obtained from the above indicated conditions.

The horizontal set-up showed clear advantages since solvent dropping was clearly avoided and consequently voltage could be reduced to more conventional values (i.e., 30 kV). In addition, a high polymer concentration could be used allowing to decrease the collection time and to get fibers with high diameter if necessary. Main limitations corresponded, in this event, to bead formation as shown in Figure 5a for a chloroform solution. Note that the increase of the polymer concentration from 17 *w*/*v*-% to 19 *w*/*v*-% allowed to avoid completely the formation of beads as clearly observed in the SEM micrographs of Figure 6. Continuous fibers with a smooth surface, a preferred orientation (see yellow arrow) and a relatively low diameter distribution (i.e., 7 ± 1.2 µm) were attained. This kind of fibers could also be obtained with the other assayed solvents using similar conditions as shown in Figure 5c for fibers coming from the electrospinning of HFIP solutions. Underline that, the high polymer concentration (i.e., 18-19 *w*/*v*-%) rendered fibers with diameters in the micron ~~area~~ scale that was considered appropriate for further biological studies.

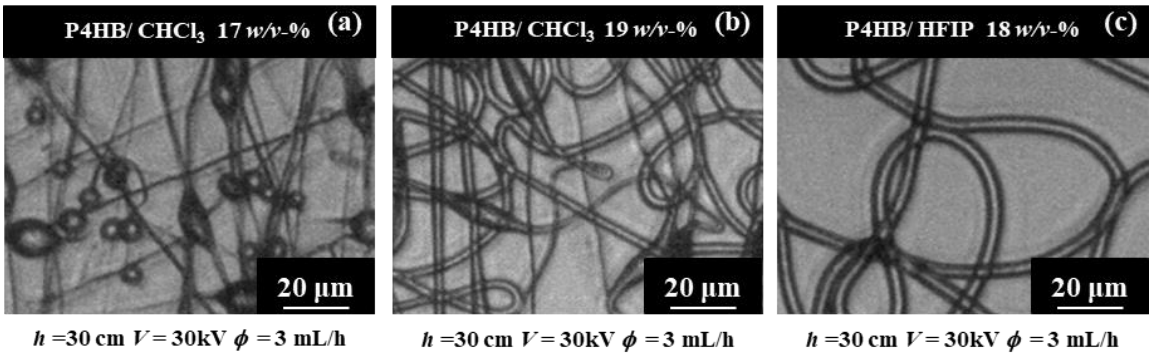

Figure 5. Optical micrographs of electrospun P4HB fibers prepared with an horizontal set up and a rotatory collector from the indicated solvent, polymer concentration, flow rate, voltage and tip-collector distance.

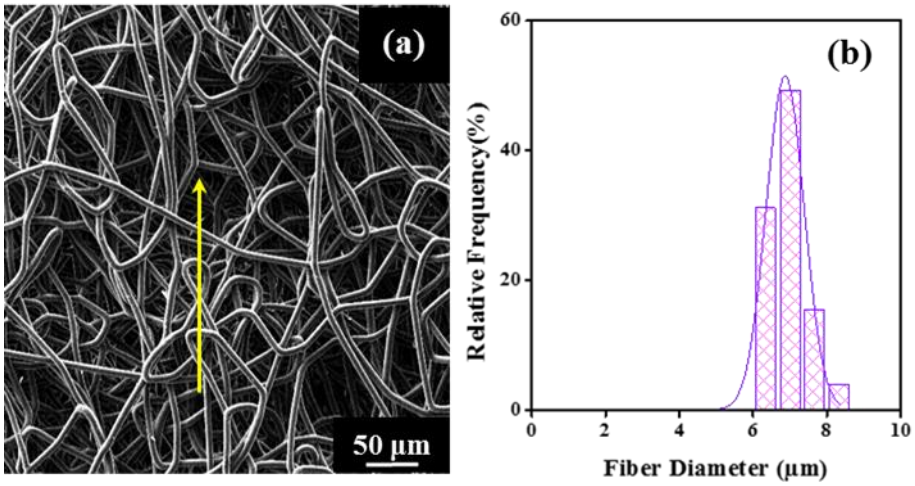

Figure 6. (a) SEM micrograph of electrospun P4HB fibers prepared from chloroform (19 *w*/*v*-%, 3 mL/h, 30 kV, 30 cm) by using horizontal electrospinning set-up. (b) Diameter distribution of electrospun fibers obtained from the above indicated conditions.

Electrospinning of P4HB solutions containing the FGF-P growth factor

Horizontal electrospinning was selected to get FGF-P loaded scaffolds due to the possibility to work with higher polymer concentration and get 3D scaffolds in a suitable period. Furthermore, a fiber diameter in micrometric scales was considered the most appropriate to encapsulate the selected growth factor. The main problem was derived from the insolubility of FGF-P in chloroform. Nevertheless, this solvent was chosen instead of HFIP due to its

lower capability to induce polyester and polypeptide degradation and more important its lower retention in the processed fibers. FGF-P could be dissolved in dimethylsulfoxide (DMSO) and consequently the electrospun solution was performed by using a 98:2 mixture of P4HB dissolved in chloroform at the 12.9 wt-% concentration and FGF-P dissolved in DMSO at a concentration of 0.9 wt-%. Therefore, the final solvent mixtures had 11.3 wt-% of P4HB and 0.001 wt-% FGF-P, respectively. P4HB scaffolds were consequently loaded with a 0.01 wt-% of FGF-P.

The influence of DMSO on the electrospinning process was evaluated using P4HB as a control. Figure 7 revealed that desirable fiber characteristics (continuity, regularity and absence of defects) were still observed without any modification of the above determined set of parameters. The main change was the reduction of the average fiber diameter (i.e., from 6.9 $\pm$ 0.02 μm for the $CHCl_3$ solution to 5.0 $\pm$ 0.05 μm for the $CHCl_3$+DMSO solution with or without FGF-P added), which could be explained by considering the increase of solution conductivity when the more polar DMSO solvent was added. Additionally, note its higher Hildebrand parameter (12.9 $(cal/mL)^{1/2}$) and its higher polar (8.07 $(cal/mL)^{1/2}$) and hydrogen bonding (4.99 $(cal/mL)^{1/2}$) Hansen contributions with respect to $CHCl_3$.

Morphologies of unloaded and FGF-P loaded electrospun P4HB fibers were practically identical (Figures 7a and 7b). SEM micrographs of loaded fibers revealed a smooth surface without any possible surface defect attributable to the incorporated growth factor.

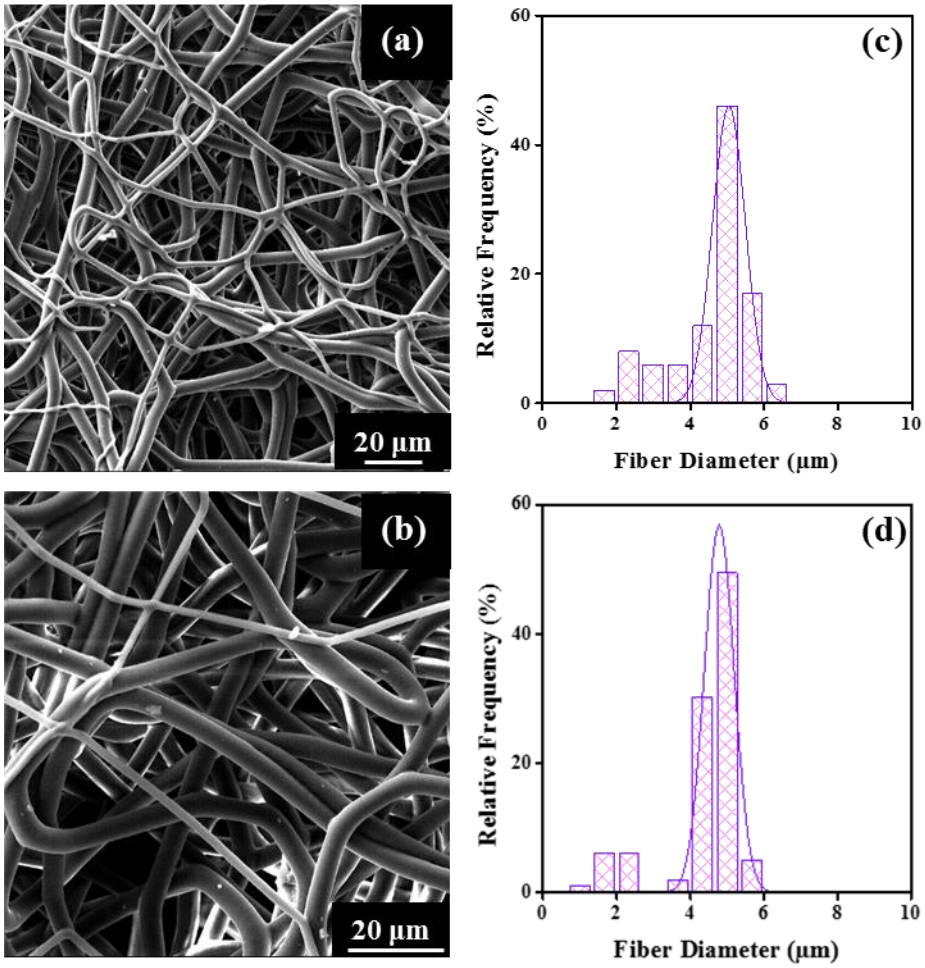

Figure 7. SEM micrographs of electrospun P4HB fibers without (a) and with the FGF-P growth factor (b). Fibers were obtained with a horizontal setup and using a $CHCl_3$+DMSO solvent mixture under the optimized conditions. The corresponding diameter size distributions are shown in (c) and (d).

Characterization of neat and FGF-P loaded P4HB electrospun scaffolds

Electrospun scaffolds of P4HB were rather crystalline, as observed from the corresponding DSC heating runs (Figure 8). Basically, a complex double melting peak was observed as consequence of the reported lamellar reordering process of P4HB that took place during the heating run and where the thinner lamellae became thicker [22, 34]. At any rate, thermal behaviour of the different scaffolds was clearly different to that observed for processed commercial sutures, which showed higher melting enthalpies and temperatures (Figure 8a).

Even the high temperature melting peak of sutures is complex as a consequence of a careful and specific procedure to process them. This consists on performing a series of heating and stretching steps carried out in order to improve mechanical properties of the final product and that clearly lead to a non-usual high melting temperature (i.e., the peak can be observed around 72 ºC). By contrast, the behaviour of a melt crystallized film is completely different to that of the initial suture and becomes characterized by a minor peak around 50 ºC and a main peak at 58 ºC, which corresponds to the reordered lamellae [22].

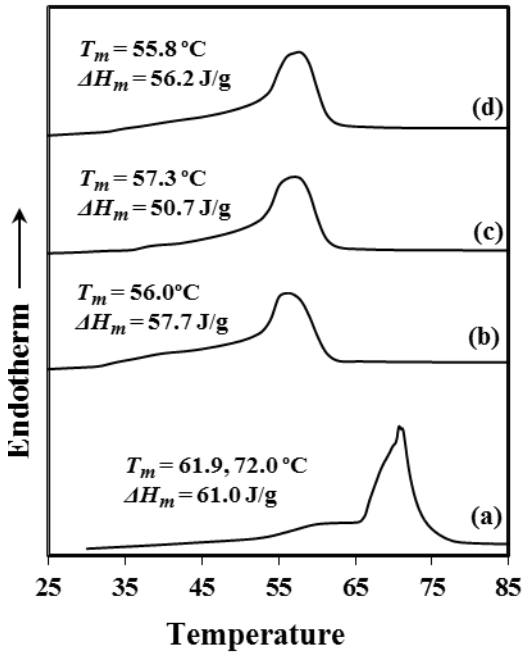

Figure 8. DSC first heating runs of: The commercial suture (a), P4HB electrospun scaffolds from $CHCl_3$ (b), $CHCl_3$/DMSO solvent mixture and $CHCl_3$/DMSO solvent mixture containing FGF-P (d).

Scaffolds coming from $CHCl_3$ solution (Figure 8b) showed two practically overlapped peaks around 56-58 ºC that suggest a greater thermodynamic stability of the thin lamellae that hinders the reordering process. In fact, the two peaks appeared well differentiated (i.e., 54.3 ºC and 59.8 ºC) and the intensity of the first one was clearly higher when the scaffold was prepared from the $CHCl_3$:DMSO mixture (Figure 8c). Minor differences on the fiber morphology (bear in mind that the diameter decreased from 6.9 to 5 μm when DMSO was

added to the $CHCl_3$ solution) seem to slightly influence on thermal properties. Figure 8d shows that scarce differences on the melting behaviour could be observed when the low amount of the growth factor was incorporated onto the scaffold.

Enthalpy values demonstrated also that P4HB was able to crystallize during the electrospinning process since a decrease of only 5% was detected with respect to the value found for the commercial suture (i.e., 57.7 J/g with respect to 61 J/g). Crystallinity slightly depended on the electrospinning conditions and the enthalpy decreased for example to 53.3 J/g (i.e., around 12%) when the $CHCl_3$:DMSO mixture was employed. The presence of the growth factor did not significantly influence on the final crystallinity.

WAXD patterns of electrospun scaffolds revealed also their crystalline character and the existence of a single crystalline form. The observed Bragg peaks appeared at 0.406 and 0.388 nm and corresponded to the (110) and (200) reflections of the reported orthorhombic structure of P4HB (*a* = 0.775 nm, b = 0.477 nm, and c (fiber axis) = 1.199 nm) [35]. The diffraction pattern also shows a significant and broad halo centered at 0.421 nm that is indicative of the amorphous content.

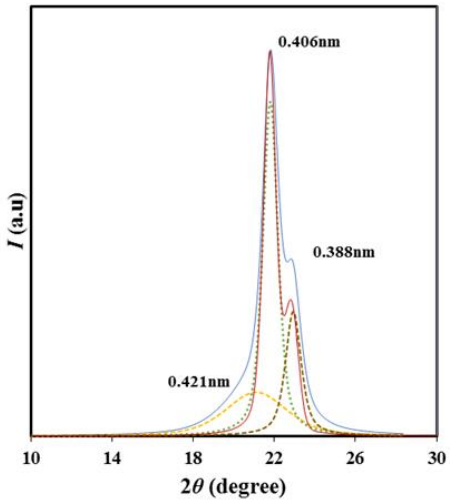

Figure 9. WAXD profile and deconvoluted peaks of P4HB electrospun scaffolds.

SAXS diffraction patterns of electrospun samples revealed also the crystalline order and the existence of supramolecular structure. The corresponding lamellar parameters being

possible to determine (i.e., long period, L_γ, amorphous layer thickness, l_a, and crystalline lamellar thickness, l_c) and crystallinity (i.e., crystallinity within the lamellar stacks, $X_c^{SAXS} = l_c/L_\gamma$) were determined by the normalized one-dimensional correlation function [36], $\gamma(r)$:

$$\gamma(r) = \int_0^\infty q^2 I(q) \cos(qr) dq / \int_0^\infty q^2 I(q) dq \qquad (2)$$

where $I(q)$ is the intensity at each value of the scattering vector ($q = [4\pi/\lambda] \sin \theta$), r the real space distance, λ the wavelength and θ the Bragg angle.

Figure 10 compares both SAXS peaks and correlation functions obtained from the representative loaded electrospun scaffold and the commercial P4HB suture. Three points should be emphasized: (a) Lamellar long period was significantly lower for the electrospun sample (i.e., 8.9 nm with respect to 10.5 nm), which is consequence of the fact that fibers were obtained at room temperature whereas the sutures were submitted as indicated to different thermal treatments that lead to reordering processes with the subsequent increase of the lamellar thickness. (b) Maximum and minimum peaks of the correlation function were better defined for the commercial suture, which means a higher electronic contrast between amorphous and crystalline phases. (c) Crystalline lamellar thickness was similar for both samples (i.e., 7.2 nm and 7.9 nm for the scaffold and the suture, respectively), whereas the amorphous lamellar thickness was rather different (i.e., 1.7 nm and 2.6 nm for the scaffold and the suture, respectively). In this way, the folding surface was more compact in the electrospun fibers in agreement with the indicated lower electronic contrast. Crystallinity in the lamellar stacks was therefore slightly higher for the electrospun fibers (i.e., 80.9% with respect to 75%)

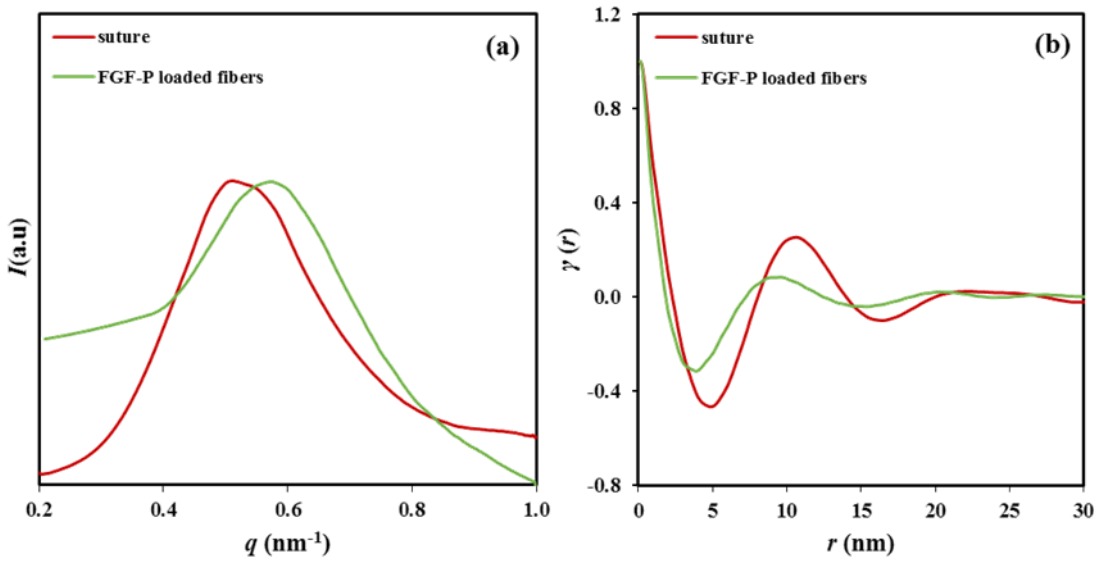

Figure 10. (a) SAXS profiles and (b) correlation functions of the commercial P4HB suture (red line) and the FGF-P loaded electrospun scaffold (green line).

Electrospun scaffolds showed good mechanical properties as consequence of their compact and tangled fibrous structure, the relative high crystallinity of the processed polymer and specially the above indicated elastic nature of P4HB. Figure 11 displays typical stress-strain curves, which are characterized by a first region of high modulus and non-plastic deformation and a second region with a low slope and high plastic deformations (i.e., even higher than 600%). Scaffolds processed under different conditions showed a variation on properties that are mainly dependent on the final diameter. Thus, fibers of 6.9 μm coming from chloroform showed greater resistance and low deformation than those with 5 μm coming from the $CHCl_3$:DMSO mixture (i.e., 28 MPa and 360% with respect to 17 MPa and 750%). Elastic moduli of the first elastic region were comparable (i.e., around 4 MPa), but significant differences were detected between the limit strengths (i.e., 12 and 6 MPa). The incorporation of the reduced amount of the FGF-P growth factor had only a slight influence on the plastic deformation that led to a slight decrease of the maximum stress (i.e., 17 MPa with respect to 15 MPa) and the maximum deformation (i.e., 730% respect to 750%) as shown also in Figure 11.

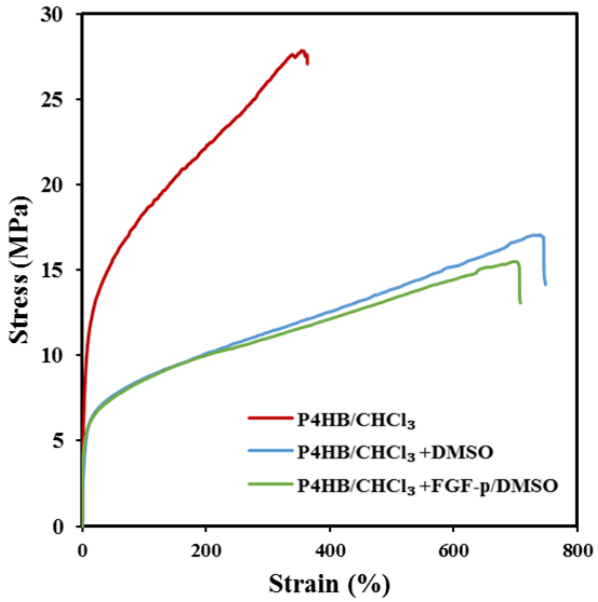

Figure 11. Stress-strain curves of selected P4HB electrospun scaffolds.

Electrospun scaffolds had a thermal stability up to temperatures more than 150 ºC higher than the melting temperature of P4HB as shown in the representative TGA curves of Figure 12. Polymer degradation seemed to follow a single decomposition step as observed in the corresponding DTGA curves. Therefore, stability of scaffolds was similar independently of the processing conditions (i.e., melt of electrospinning) and the incorporation of the growth factor.

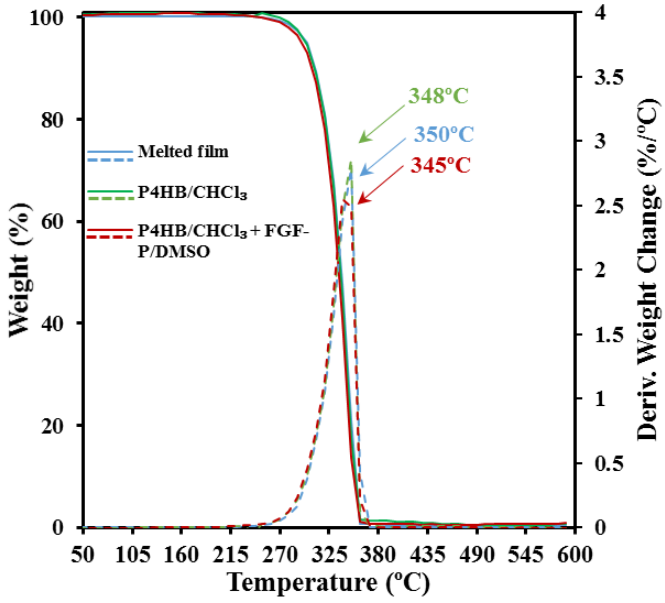

Figure 12. TGA (solid lines) and DTGA (dashed lines) curves of the indicated P4HB samples. Note that the curve of the melted film overlaps the curves of the electrospun nanofibers.

Surface characteristics are a primordial property of materials when they should be employed for tissue engineering applications. In overall, it is assumed that serum-treated hydrophilic surfaces support significantly greater cell attachment, cell spreading, and cytoskeletal organization relative to hydrophobic surfaces [37]. Contact angle measurements of the prepared scaffolds displayed a slight hydrophobicity with angles around 105º (Figure 13). These values were higher than detected for the original suture (85º) and even for a smooth melt casting film (73º). Probably, the increase on the surface roughness of the scaffolds [38] and the higher contribution of air pockets [39] were the reason of the observed increase on the hydrophobicity. Angles slightly decreased by the reduction of the microfiber diameter as observed when scaffolds from $CHCl_3$ and $CHCl_3$ + DMSO are compared. Most significantly, a clear angle shift towards a more hydrophobic value (121º) was detected when the peptide growth factor was loaded.

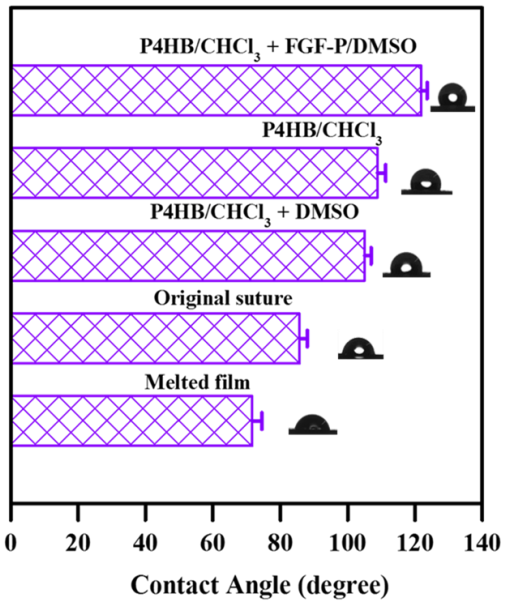

Figure 13. Contact angle measurements of P4HB electrospun scaffolds in distilled water and comparison with the original suture.

***In-vitro* wound healing activity**

The *in-vitro* wound-healing assay, also known as the scratch assay is a helpful alternative to animal models where a complete wound-closure research can be performed. The *in-vitro* wound healing assay study the proliferation and migration of cells. Specifically, the assay measures at the microscopic scale the rate at which cells, in a cell monolayer, migrate to fill a cell-free gap homemade by a scratch [40]. Initially, primary cultures of epithelial and endothelial cells were used in this assay. However, the cell lines derived from embryo, normal and tumor tissues are frequently used for getting a better control of culture cell growth [41, 42]. For example, MC-3T3 cells (fibroblasts derived from mouse embryo) [43], HUVEC cells (normal endothelial cells isolated from human umbilical vein) [44], HaCaT cells (cell line that is a spontaneously transformed aneuploidy immortal keratinocyte cell line from adult human skin) [45], HEK-293 cells (epithelial cells isolated from human embryonic kidney, immortal cells that contain adenovirus and forms tumors in nude mice) [46], and others line cells derived from tumor: 769-P cells (human renal carcinoma cell line) [40], Py4-1 cells (hemangioendothelioma cells) [47], MCF-7 cells (epithelial mammary carcinoma cells) [48], etc. Note that the main requisite of the cells used in this assay is the capability to render a 2D-growth with formation of a cell monolayer or a cell sheet [42].

The activity of FGF-P for wound healing was demonstrated *in-vitro* by evaluating the growth of Saos-2 epithelial-like and NRK fibroblasts-like cells. The FGF-P was tested at doses of 0.0003, 0.002, 0.003 and 0.02 mg/mL, to this end the synthetic factor was diluted from a stock of 1 mg/mL (prepared in PBS) in 1 mL of culture medium. Figure 14a shows that both cell types grow in a dose-dependent manner with an increase in the number of cells when they were stimulated with FGF-P. The increased cell growth is shown normalized according to the control that corresponds to a nil FGF-P dose. However,

growth was significantly higher in NRK fibroblasts. This result was expected since the synthetic factor FGF-P was designed based on FGF-2, which binds naturally to its receptor (FGFR1) in fibroblasts and stimulates the proliferation, migration and cell differentiation [21, 49]. Recently, it has been described that osteoblasts are stimulated with FGF-2 during their transition and differentiation to osteoclast [50]. Therefore, it can be justified that Saos-2 cells of bone origin showed an increase in their cell population in response to the FGF-P stimulus. Namely, Saos-2 cells were not totally refractory to the influence of FGF-P despite giving rise to a lower response than that found for NRK fibroblasts.

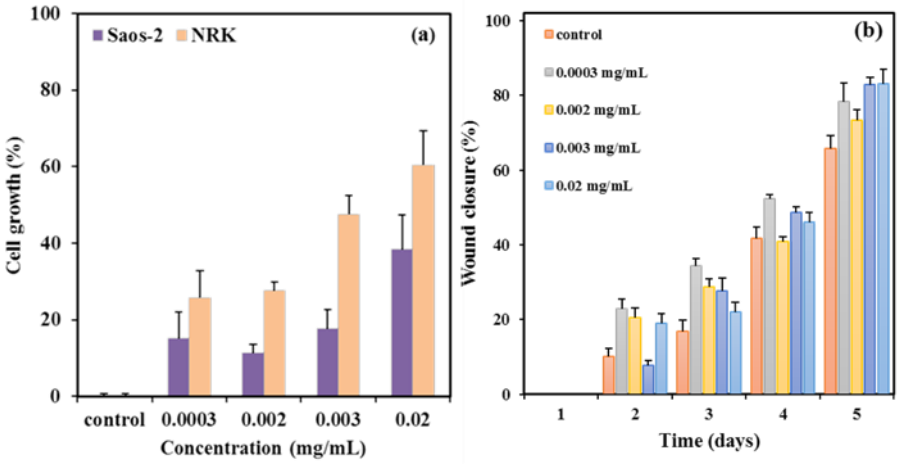

Figure 14. (a) Dose-response effect of the synthetic factor FGF-P on cell proliferation (96 hours). *In-vitro* evolution of wound healing during culture time and different doses of FGF-P (b).

Figure 14b shows the time-course during the culture of the NRK fibroblasts exposed to different doses of FGF-P. Initially, the lower doses (0.0003 and 0.002 mg/mL) seem to be more stimulating for proliferation (e.g., second and third day of culture), while the higher doses (0.003 and 0.02 mg/mL) could be responsible for a negative regulation of the receptor through the typical mechanisms of regulation of membrane receptors, such as internalization and degradation [49, 51, 52]. However, in prolonged culture times

(fourth and fifth day of culture) it is observed that high doses (such as, 0.003 and 0.02 mg / mL) were more stimulatory for cell growth. In addition, at the above mentioned times of culture it seems that both doses achieve a similar cellular response as a saturation effect. For this reason, the dose of 0.003 mg/mL was selected as the loading dose in the P4HB fiber matrix.

In-vitro biocompatibility of P4HB electrospun scaffolds with the indicated FGF-P load was determined by adhesion and proliferation assays using NRK cells (Figure 15). Fibroblasts were specifically selected since their adhesion to material surfaces implied focal joint points instead of the wide extension of cell membrane that is characteristic of the epithelial cells. Figure 15a shows that the adhesion after 24 h of the NRK cells on the fiber scaffolds (3D growth) was greater than on the 2D surface of the well. The improved adhesion of the NRK cells in the fiber scaffold is due to the micrometric diameter of the fibers and the more hydrophilic character (i.e., with respect to the control) of the scaffold. However, at 96 hours of culture (i.e., the proliferation event) a lower percentage of the number of cells was observed in the scaffolds loaded with FGF-P and an increase of about 20% was observed in the well (Figure 15b). This result can be explained by indicating that the FGF-P diffuses from the matrix to the medium and therefore the entire population of cells contained in the well becomes stimulated.

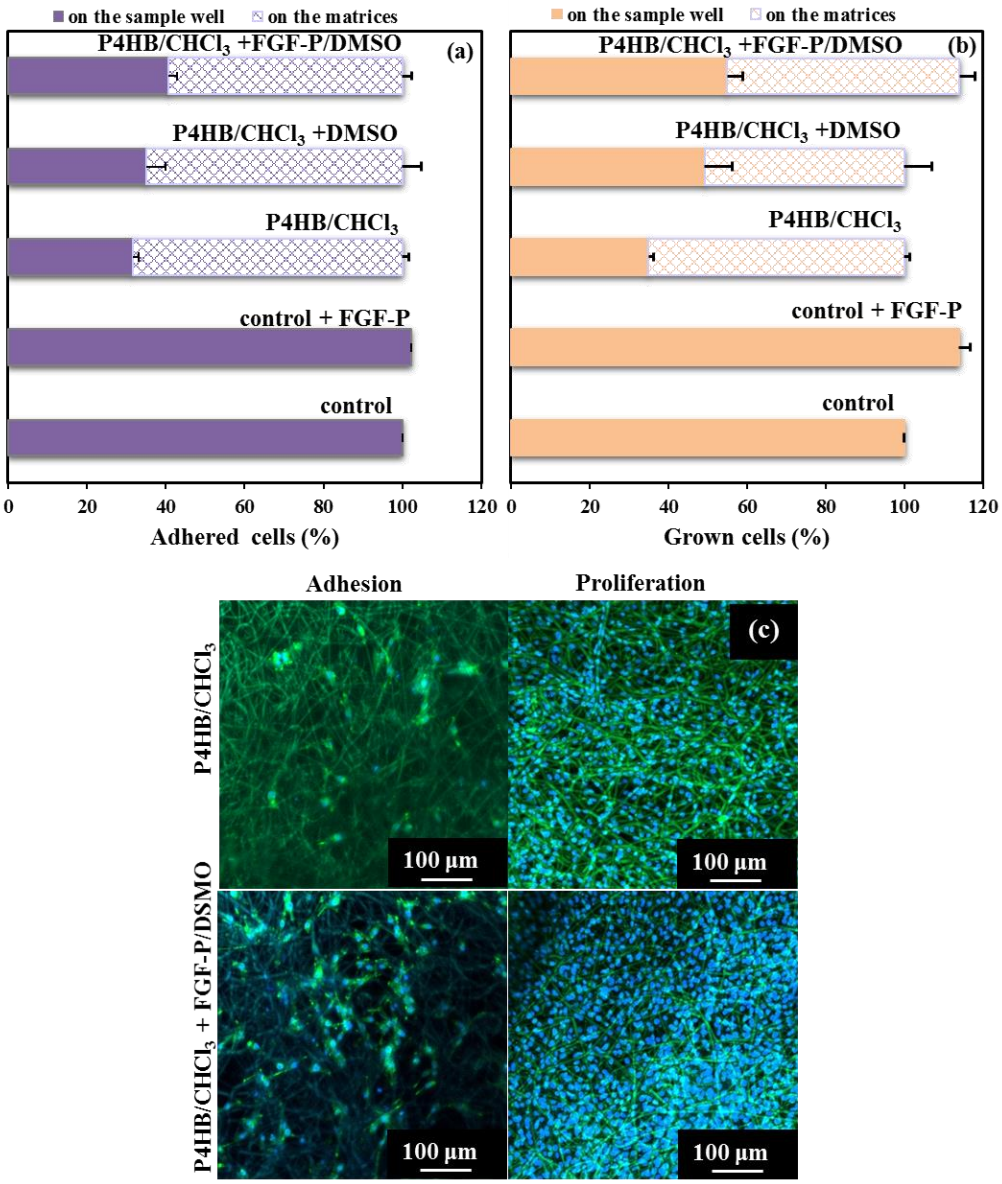

Figure 15. Adhesion (a) and proliferation (b) of fibroblast-like NRK cells on the different samples of the P4HB electrospun scaffolds. (c) Fluorescence microscopy images showing the adhesion and proliferation of NRK cells in P4HB electrospun scaffolds with and without the FGF-P load.

Finally, the fluorescence microscopy images (Figure 15c) illustrate the high biocompatibility of loaded scaffolds compared to neat scaffolds. It could be concluded that the fiber matrices are suitable supports for both adhesion and proliferation of cells, and do not have cytotoxic effects for the cells growing in the matrices.

The results of the study of *in-vitro* wound healing in the presence of electrospun scaffolds loaded with FGF-P are shown in Figure 16. We consider that this test is the gold standard to demonstrate the applicability of these scaffolds. Thus, it allows to verify that the incorporated FGF-P is conveniently released from the matrices into the medium, and that it can stimulate cell proliferation.

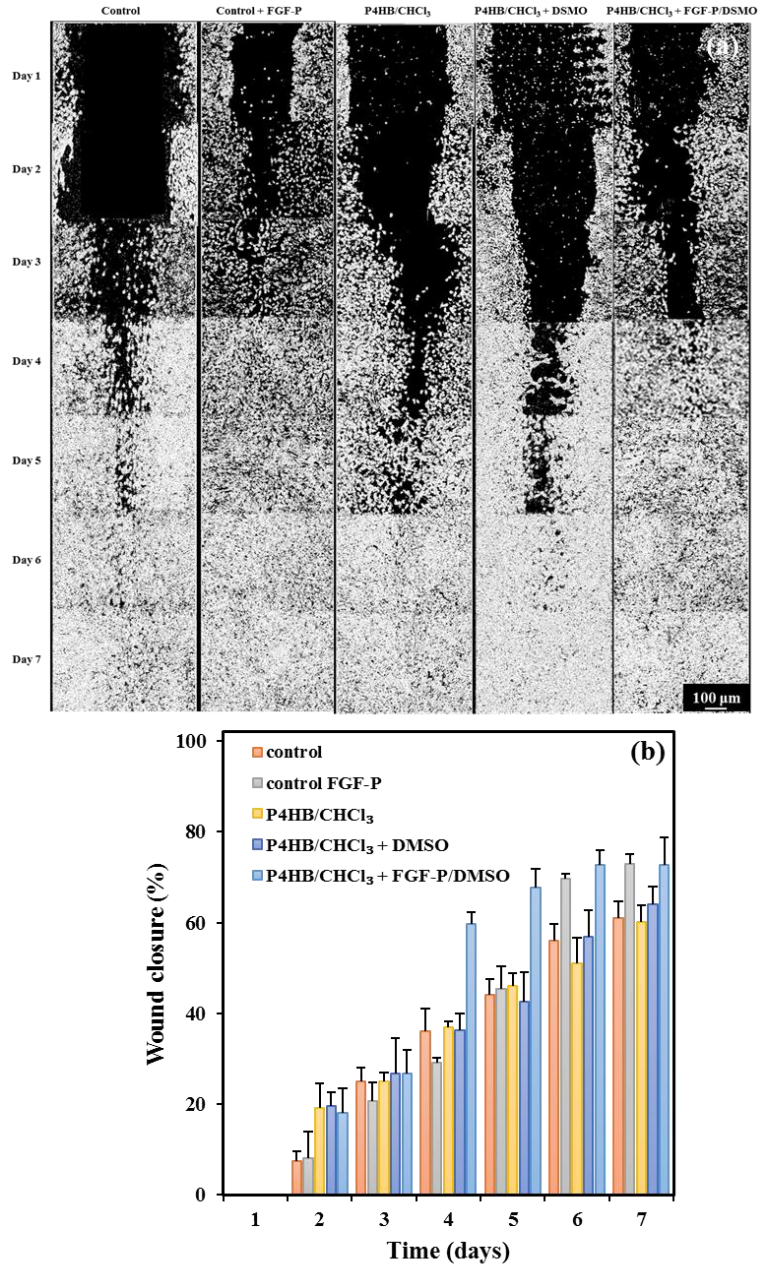

Figure 16. Optical microscopy images of the *in-vitro* wound healing evolution in the presence of the different P4HB electrospun matrices (a). Quantification of the cellular

colonization of the scratch during the time evolution of the *in-vitro* wound healing assay (b).

Figure 16a depicts the light microscopy images corresponding to the scratch healing process in the presence of the P4HB electrospun scaffold loaded with the synthetic factor FGF-P and the respective controls. The scratch can clearly be observed up to the third day of culture in the control conditions (growth in culture medium) and in the growth conditions of the cells in the presence of the unloaded electrospun scaffolds (e.g., P4HB-$CHCl_3$ and P4HB-$CHCl_3$ + DMSO). On the other hand, the P4HB electrospun loaded with FGF-P as well as the control + FGF-P (culture medium supplemented with FGF-P) showed a clear imprint of the scratch until only the second day of culture, namely the presence of FGF-P accelerates scratch healing. The mechanism of the process simply corresponds to the increase in the cells number caused by the presence of the growth factor FGF-P. Finally, it can be observed that after the fifth day of culture, the morphological scratch healing occurs in all the conditions studied.

The quantitative data (Figure 16b) on the growth of NRK fibroblasts during scratch healing demonstrate a linear increase for the control and for the two non-loaded electrospun scaffolds (i.e., P4HB/$CHCl_3$ and P4HB/$CHCl_3$ + DMSO). Scratch healing in the control supplemented with FGF-P initially occurred according to a linear NRK growth, but an exponential change was observed between the fifth and sixth day of culture. However, the scratch healing in the presence of the electrospun scaffold loaded with FGF-P was the fastest condition since the exponential growth was observed between the third and fourth day of culture. These quantitative data are clearly consistent with the qualitative description based on the light microscopy images. In this sense, it can be concluded that the progressive release of FGF-P from the electrospun scaffold favours the stimulation of the growth of NRK fibroblasts in comparison to its application as a bolus in cell culture.

CONCLUSIONS

Electrospun scaffolds of P4HB were successfully obtained from different solvents after cautious optimization of polymer concentration and electrospinning parameters. Drop formation, fiber agglomeration and solvent retention where the main observed problems. In general terms, chloroform resulted the most appropriate solvent to get continuous, uniform and smooth microfibers. The equipment with a horizontal set-up configuration was appropriate to solve drop formation problems, while allowing to work with high flow rates and polymer concentrations.

The processing under the optimized conditions led to semicrystalline microfibers (i.e., diameters around 7 μm) with lower lamellar thickness and melting point than the commercial suture submitted to thermal and stretching treatments. Electrospun scaffolds showed excellent mechanical properties with Young modulus, maximum strength and elongation values of 4 MPa, 28 MPa and 360%, respectively and surfaces with higher hydrophobic character than initial sutures due to an increase on the roughness.

The FGF-P peptide growth factor was successfully loaded into the P4HB scaffolds by the modification of the electrospinning solvent. The required addition of a small DMSO percentage led to a slight decrease of the fiber diameter and a change on the scaffold properties. Specifically, the maximum strength decreased and the elongation at break (i.e., from 360% to 730%) increased. Loaded samples showed a good biocompatibility, a slight hydrophobicity and a clear wound healing effect when the amount of incorporated FGF-P was 0.01 wt-%. Finally, the new fiber scaffold may have promising biomedical applications in tissue engineering and reparative medicine by reducing the time required for wound closure.

Acknowledgements

The authors are in debt to support from MINECO and FEDER (RTI2018-101827-B-I00) and the Generalitat de Catalunya (2017SGR373). I.K. acknowledges also the financial support from B. Braun Surgical S.A.U. Diffraction experiments were performed at the NCD-SWEET beamline at ALBA Synchrotron with the collaboration of ALBA staff.

REFERENCES

[1] D.P. Martin, S.F. Williams, *Biochem. Eng. J*. 2003, **16**, 97

[2] J. uwe Ackermann, S. Müller, A. Lösche, T. Bley, W. Babel, *J. Biotechnol*. 1995, **39**, 9.

[3] S. Ferrara, S. Zotti, L. Tedeschi, G. Frison, F. Castagna, L. Gallimberti, G. Gessa, P. Palatini, Br. *J. Clin. Pharmacol*. 1992, **34**, 231.

[4] P4HB made TephaFLEX is our breakthrough Technology, https://www.tepha.com/technology/overview/, accessed April 17, **2020**.

[5] E.K. Odermatt, L. Funk, R. Bargon, D.P. Martin, S. Rizk, S.F. Williams, *Int. J. Polym. Sci*. 2012, **2012**, 1.

[6] Tornier, announces launch of BioFiber® Surgical Mesh for tendon repair at arthroscopic surgery conference, Tornier Press Release. https://www.businesswire.com/news/home/20110414005940/en/Tornier-Announces-Launch-BioFiber®-Surgical-Mesh-Tendon, accessed July 2, **2020**.

[7] C.R. Deeken, B.D. Matthews, *ISRN Surg*. 2013, **2013**, 1.

[8] S.F. Williams, S. Rizk, D.P. Martin, *Biomed. Eng*. 2013, **58**, 439.

[9] D.H. Reneker, I. Chun, *Nanotechnology*. 1996, **7**, 216.

[10] D. Li, Y. Xia, *Adv. Mater*. 2004, **16**, 1151.

[11] J.M. Deitzel, J. Kleinmeyer, D. Harris, N.C.B. Tan, *Polymer*. 2001, **42**, 261.

[12] G. Yang, X. Li, Y. He, J. Ma, G. Ni, S. Zhou, *Prog. Polym. Sci*. 2018, **81**, 80.

[13] L. Li, G. Zhou, Y. Wang, G. Yang, S. Ding, S. Zhou, *Biomaterials*. 2015, **37**, 218.

[14] G. Yang, J. Wang, Y. Wang, L. Li, X. Guo, S. Zhou, *ACS Nano*. 2015, **9**, 1161.

[15] E. Llorens, L.J. Del Valle, J. Puiggalí, *J. Appl. Polym. Sci*. 2016, **133**, 1.

[16] D.P. Martin, A. Badhwar, D. V. Shah, S. Rizk, S.N. Eldridge, D.H. Gagne, A. Ganatra, R.E. Darois, S.F. Williams, H.C. Tai, J.R. Scott, *J. Surg. Res*. 2013, **184**, 766.

[17] C. Sanhueza, F. Acevedo, S. Rocha, P. Villegas, M. Seeger, R. Navia, *Int. J. Biol. Macromol*. 2019, **124**, 102.

[18] T. Volova, D. Goncharov, A. Sukovatyi, A. Shabanov, E. Nikolaeva, E. Shishatskaya, *J. Biomater. Sci. Polym. Ed*. 2014, **25**, 370

[19] Y. Shing, J. Folkman, R. Sullivan, C. Butterfield, J. Murray, M. Klagsbrun, *Science*. 1984, **223**, 1296.

[20] M. Goldfarb, *Cytokine Growth Factor Rev*. 1996, **7**, 311.

[21] K. Casey-Sawicki, M. Zhang, S. Kim, A. Zhang, S.B. Zhang, Z. Zhang, R. Singh, S. Yang, S. Swarts, S. Vidyasagar, L. Zhang, A. Zhang, P. Okunieff, *Health Phys*. 2014, **106**, 704.

[22] I. Keridou, L.J. del Valle, L. Funk, P. Turon, I. Yousef, L. Franco, J. Puiggalí, *Polym. Morphol. Princ. Charact. Process*. 2019, **12**, 1.

[23] E. Llorens, L.J. Del Valle, A. Díaz, M.T. Casas, J. Puiggalí, *Macromol. Res*. 2013, **21**,

775.

[24] S. Preibisch, S. Saalfeld, P. Tomancak, *Bioinformatics*. 2009, **25**, 1463.

[25] C. Yang, Z. Jia, Z. Xu, K. Wang, Z. Guan, L. Wang, *Annu. Rep. - Conf. Electr. Insul. Dielectr. Phenomena, CEIDP*. 2009, 204.

[26] M.G. McKee, C.L. Elkins, T.E. Long, *Polymer*. 2004, **45**, 8705.

[27] C.J. Luo, M. Nangrejo, M. Edirisinghe, *Polymer*. 2010, **51** 1654.

[28] D.W. Van Krevelen, K.T. Nijenhuis, *Cohesive properties and solubility*, 4th ed., Elsevier B.V, Amsterdam, The Netherlands, **2009**.

[29] C.M. Hansen, *The three dimensional solubility parameter and solvent diffusion coefficient. Their importance in surface coating formulation*, Danish Tecnhical Press, Copenhagen, **1967**.

[30] M. Terada, R.H. Marchessault, *Int. J. Biol. Macromol*. 1999, **25**, 207.

[31] D.M. Correia, C. Ribeiro, J.C.C. Ferreira, G. Botelho, J.L.G. Ribelles, S. Lanceros-Mendez, V. Sencadas, *Polym. Eng. Sci*. 2013, **54**, 1608.

[32] C.M. Hansen, *Hansen solubility parameters: A user's handbook*: Second edition, CRC Press, Boca Raton, FL, USA, **2007**.

[33] N. Jacquel, C.-W. Lo, H.-S. Wu, S.S. Wang, *AIChE J*. 2007, **53**, 2704.

[34] R. Alamo, L. Mandelkern, *J. Polym. Sci. Part B Polym. Phys*. 1986, **24**, 2087.

[35] F. Su, T. Iwata, K. Sudesh, Y. Doi, *Polymer*. 2001, **42**, 8915.

[36] C.G. Vonk, G. Kortleve, *Kolloid-Zeitschrift Zeitschrift Für Polym*. 1967, **220**, 19.

[37] K. Webb, V. Hlady, P.A. Tresco, *J. Biomed. Mater. Res.* 1988, **41**, 422.

[38] R.N. Wenzel, *Ind. Eng. Chem.* 1936, **28**, 988.

[39] B.D. Cassie, S. Baxter, *Trans. Faraday Soc.* 1944, 546.

[40] A.V.P. Bobadilla, J. Arévalo, E. Sarró, H.M. Byrne, P.K. Maini, T. Carraro, S. Balocco, A. Meseguer, T. Alarcon, *J. R. Soc. Interface.* 2019, **16**.

[41] C.C. Liang, A.Y. Park, J.L. Guan, *Nat. Protoc.* 2007, **2**, 329.

[42] J.E.N. Jonkman, J.A. Cathcart, F. Xu, M.E. Bartolini, J.E. Amon, K.M. Stevens, P. Colarusso, *Cell Adhes. Migr*. 2014, **8**, 440.

[43] A. Lipton, I. Klinger, D. Paul, R.W. Holley, *Proc. Natl. Acad. Sci. U. S. A.* 1971, 68, 2799.

[44] P.Y.K. Yue, E.P.Y. Leung, N.K. Mak, R.N.S. Wong, *J. Biomol. Screen*. 2010**, 15,** 427.

[45] S. Liarte, Á. Bernabé-García, D. Armero-Barranco, F.J. Nicolás, *J. Vis. Exp.* 2018, **2018**, 1.

[46] B. Tanno, F. Sesti, V. Cesi, G. Bossi, G. Ferrari-Amorotti, R. Bussolari, D. Tirindelli, B. Calabretta, G. Raschellà, *J. Biol. Chem.* 2010, **285**, 29434.

[47] T. Gebäck, M.M.P. Schulz, P. Koumoutsakos, M. Detmar, TScratch: *Biotechniques*. 2009, **46**, 265.

[48] N.A. Razak, N. Abu, W.Y. Ho, N.R. Zamberi, S.W. Tan, N.B. Alitheen, K. Long, S.K.

Yeap, S*ci. Rep.* 2019, **9**, 1.

[49] V.P. Eswarakumar, I. Lax, J. Schlessinger, *Cytokine Growth Factor Rev.* 2005, **16**, 139.

[50] C.M. Teven, E.M. Farina, J. Rivas, R.R. Reid, *Genes Dis*. 2014, **1**, 199.

[51] D.M. Ornitz, N. Itoh, *Genome Biol*. 2001, **2**, reviews3005.1.

[52] D.M. Ornitz, N. Itoh, *Wiley Interdiscip. Rev. Dev. Biol*. 2015, **4**, 215.